Perfusable cell-laden matrices to guide patterning of vascularization *in vivo*

Siavash Parkhideh[1], Gisele A. Calderon[1], Kevin D. Janson[1], Sudip Mukherjee[1], A. Kristen Mai[1], Michael D. Doerfert[1], Zhuoran Yao[1], Daniel W. Sazer[1], Omid Veiseh[1,#]

[1]Department of Bioengineering, Rice University, Houston, TX 77030, USA

[#]Corresponding author:
Omid Veiseh, PhD
Rice University
Department of Bioengineering
6500 Main Street, Suite 523
Houston, Texas 77030
omid.veiseh@rice.edu

Abstract

The survival and function of transplanted tissue engineered constructs and organs require a functional vascular network. In the body, blood vessels are organized into distinct patterns that enable optimal nutrient delivery and oxygen exchange. Mimicking these same patterns in engineered tissue matrices is a critical challenge for cell and tissue transplantation. Here, we leverage bioprinting to assemble endothelial cells in to organized networks of large (>100μm) diameter blood vessel grafts to enable spatial control of vessel formation in vivo. Acellular PEG/GelMA matrices with perfusable channels were bioprinted and laminar flow was confirmed within patterned channels, beneficial for channel endothelialization and consistent wall shear stress for endothelial maturation. Next, human umbilical vein endothelial cells (HUVECs) were seeded within the patterned channel and maintained under perfusion culture for multiple days, leading to cell-cell coordination within the construct *in vitro*. HUVEC and human mesenchymal stromal cells (hMSCs) were additionally added to bulk matrix to further stimulate anastomosis of our bioprinted vascular grafts *in vivo.* Among multiple candidate matrix designs, the greatest degree of biomaterial vascularization *in vivo* was seen within matrices fabricated with HUVECs and hMSCs encapsulated within the bulk matrix and HUVECs lining the walls of the patterned channels, dubbed design M-C_E. For this lead design, vasculature was detected within the endothelialized, perfusable matrix channels as early as two weeks and αSMA+ CD31+ vessels greater than 100 μm in diameter had formed by eight weeks, resulting in durable and mature vasculature. Notably, vascularization occurred within the endothelialized, bioprinted channels of the matrix, demonstrating the ability of bioprinted perfusable structures to guide vascularization patterns *in vivo*. The ability to influence vascular patterning *in vivo* can contribute to the future development of vascularized tissues and organs.

Keywords: bioprinting, vascularization, angiogenesis, tissue engineering, regenerative medicine

1. Introduction

Tissue engineering and regenerative medicine hold valuable promise in disease modeling, drug discovery, and organ transplantation (1-4). Over 100,000 people in the United States are on the national organ waiting list and 17 people die each day waiting for an organ (5). While significant

advances have been made in tissue engineering, including developing replenishable cell sources (6), clinical translation of many of these approaches has been hindered by the inability to develop functional vessels for tissue grafts and organs (7). The vasculature is critical for tissues to receive oxygen and nutrients and have metabolic wastes removed (7). Cells cannot maintain viability if they are greater than 100-200 μm away from a blood vessel (8) and tissues undergo central necrosis without sufficient nutrient access (9, 10), demonstrating the crucial need for vascularization. Vasculature provides additional valuable functions, including allowing immune interrogation, thermoregulation, and multi-tissue communication via hormones (7, 11), which are relevant for the function of larger and more complex organs. While capillaries have been successfully developed within many engineered tissues, a key unsolved challenge has been successfully developing large vessels with guided patterns *in vivo* (7).

Vascular patterning is essential for tissue engraftment and functionality (12-14). The bodies, natural vascular system is structured hierarchically, with large arteries branching down to arterioles and capillaries. Furthermore, specific architectural features of the vasculature are conserved among multiple species (15-17). These conserved vascular parameters may be explained by the balance of convection and diffusion needed to deliver nutrients throughout the body (16). Endothelial cells (ECs) and MSCs within biodegradable matrices are commonly used to promote matrix vascularization. MSCs specifically aid the vascularization process by secreting pro-angiogenic factors (18), degrading the local extracellular matrix (ECM) to enhance EC migration (19), and stabilizing newly formed proto-vascular structures (20, 21). These vascular structures can become integrated with the host via inosculation, reducing the duration of potential hypoxia after engineered tissue implantation (22, 23). However, much of these vessels become capillary-scale without proper control over vascular patterning (12-14). Furthermore, non-patterning approaches (24-27) and many patterning approaches including micro molding (12, 13) and self-assembly (14, 28), while showing good engraftment of therapeutic cells, primarily show capillary-scale vessel formation *in vivo* highlighting the need for larger vessel formation.

The stereolithography apparatus for tissue engineering (SLATE) bioprinting is a digital light projection (DLP) stereolithography technique that creates perfusable architectures in biocompatible materials with cells throughout the bioprinted construct (29, 30). SLATE bioprinting was used to achieve the benefits of transplanting MSCs and endothelial cells within a matrix and enable matrix patterning. SLATE bioprinting can fabricate constructs with cell-adhesive and degradable materials such as GelMA (29-33), create handle-able materials for surgical implantation (29), and create perfusable vascular networks with smooth inner surfaces for patterning endothelial cells (34-36). These beneficial aspects encouraged its use for this study.

In this study, we utilize a bioprinting approach to fabricate patterned, cell-containing matrices and evaluate the ability of these constructs to promote patterned vascularization and guide formation of larger (>100 μm) vessels in small animal models. Achieving patterned vascularization can help advance the field towards developing organs and tissues for transplantation.

2. Materials and Methods

2.1 *Materials synthesis*

Photoiniatior lithium phenyl-2,4,6-trimethylbenzoylphosphinate (LAP) was prepared as described previously (37) by reacting equimolar amounts of dimethyl phenylphosphonite and

2,3,6-trimethylbenzoyl chloride under argon overnight at room temperature, followed by the addition of 4 molar excess of lithium bromide in 2-butanone. The reaction was heated to 50°C, then cooled to room temperature for 4 hours, followed by filtration. Poly(ethylene glycol) diacrylate (PEGDA) 3.4 kDa was synthesized by the reaction between poly(ethylene glycol) and acryloyl chloride in the presence of triethylamine overnight (38). Gelatin methacrylate (GelMA) was synthesized by the dropwise addition of methacrylic anhydride (0.1 mL per 1.0 g gelatin) to the mixture of gelatin (Type A, bloom 300) dissolved in 100 mM carbonate/bicarbonate buffer (pH = 9.5) at 50°C for 4 hours (39).

2.2 *Matrix fabrication with projection stereolithography*

Monolithic matrices were fabricated with projection stereolithography (pSLA) which involves sequential crosslinking of photo-sensitive polymers in a layer-by-layer fashion via the projection of photomasks to create a 3D volume (40). Our lab has developed a custom pSLA 3D printer consisting of a commercial digital light processing (DLP) projector, a stepper motor and axis for the z-stage, a RepRap Arduino Mega Board (RAMBo), and 3D printed housing components which were fabricated using an Ultimaker 2 (Ultimaker, Netherlands) from consumer-grade poly(lactic acid) (PLA) plastic filament. The complete setup is described in reference (29). The matrices are fabricated layer-by-layer by attaching to the glass slide surface on the z-stage, which is immersed into a poly(dimethylsiloxane) (PDMS) coated (6:1 base to catalyst) vat of pre-polymer solution. The XY build size is 64x40 mm and has an XYZ resolution of 50 μm determined by the projector optics (XY) and photoabsorbers used (Z). The light source is 405 nm and is attached to a computer to control the motor, heating element, and projection of photomasks.

Pre-hydrogel mixtures were prepared to contain 3.25 wt% 3.4 kDa PEGDA, 10 wt% GelMA, 17 mM LAP, 10% glycerol, and 2.255 mM tartrazine. Tartrazine (yellow food coloring FD&C Yellow 5, E102) is used as a photoabsorber previously established as a low toxic dye that washes out easily to result in a transparent matrix for facile imaging (29). Should cells be encapsulated in the bulk of the matrix, the desired concentration and co-culture ratio of cells are included and resuspended in the pre-hydrogel solution: $5x10^6$ RFP-HUVECs (passages 7-9, AngioProteomie) and $1x10^6$ hMSCs (passages 4-8, Rooster Bio) per mL of printing solution. The pre-hydrogel mixture is loaded into the PDMS coated dish, where the build platform is lowered to the first layer position. Creation Workshop software (http://www.envisionlabs.net/) enables control over the printer with GCode commands sent for vertical movement of the z-stage, projection of the photomask sequence, and controlled heating of the heating element. Because GelMA is sensitive to thermal gelation, the vat is maintained at 37˚C to maintain an aqueous pre-hydrogel mixture until crosslinked. Each layer height was set to 50 μm with exposure times adapted for each batch of GelMA (typically between 10-15 seconds per layer) at 19.5 mW/cm^2 power output. After the printed construct is complete, the 3D matrix is removed from the glass slide by applying a razor between the matrix and the slide and allowed to swell overnight in PBS with multiple washes.

2.3 *Bead tracking*

Matrices were fabricated and mounted into 3D printed chambers to ensure stability and proper alignment of inlet and outlet. Flexible 18-gauge needle tips (Nordson) were inserted into this chamber so that the tips were firmly anchored in the patterned channel of the matrix. A 1:400

dilution of 2.1 μm red fluorescent beads (Magsphere) suspended in a 30% glycerol solution was perfused through the matrix at a rate of 5 μL/min. The flow of beads was visualized using a Ti-E inverted microscope (Nikon) and a Zyla 4.2 sCMOS camera (Andor). After establishing flow equilibrium, 100 frames of bead flow were captured with 24.6 ms of exposure per frame. This process was repeated for three different regions within the same matrix.

Image processing was performed by adapting a previously described protocol (41). Briefly, images were first modified by subtracting the minimum intensity projection of each 100-frame sequence. PIV analysis was performed using the PIVlab app (v.2.54) within MATLAB (v.R2021a). Images were contrast-enhanced via a highpass filter, and an ROI encompassing the entire channel was manually isolated. Velocity data were quantified using four passes of PIVlab's fast Fourier transform algorithm. These data were averaged over all frames of the sequence, and the resulting average velocity heatmaps are shown **(Fig. 2,c-e)**. Velocity profiles along the width of the channel were analyzed across a 1-D line roughly perpendicular to the edges of the channel. Flow velocity magnitudes were calculated along that line for all frames. Mean and standard deviation were calculated along the line and were plotted for three regions of the same matrix **(Fig. 2f)**.

2.4 *Hydrogel architecture and composition*

M-AC (matrix, acellular) and M-AC_P (matrix, acellular and perfusable) hydrogels were fabricated using bioprinted GelMA/PEGDA matrices. Three candidate matrices with ECs and MSCs in the bulk matrix were also evaluated: M-C_CC (matrix, cellularized bulk with collagen cords in the channel), M-C_E (matrix, cellularized bulk, and endothelialized channel), and M-C_EGP (matrix, cellularized bulk, and endothelialized channel with gelatin plug). M-C_E hydrogels contain ECs and hMSCs in the bulk matrix and EC-lined channels, maintaining endothelial cells under perfusion culture. M-C_EGP hydrogels were designed to be the same as M-C_E designs, except liquid gelatin was injected into the endothelialized lumen prior to implantation to form a thermoreversible plug to prevent perioperative fluid ingress into the patterned channel.

2.5 *Cell culture, channel endothelialization, matrix perfusion culture, and epifluorescence imaging*

Endothelialization perfusion was established according to a previously established protocol (30). For our application, human umbilical vein endothelial cells (HUVEC) (GFP HUVECs, AngioProteomie) were cultured in VascuLife Medium and supplements (LifeLine Technologies, Frederick, MD) at 37˚C and 5% CO_2. The matrix was placed inside a custom PLA gasket to serve as a perfusion chamber, closely fitting the gel as well as the inlet and outlet 18-gauge needle tips. Before placing the matrix, the chamber was bonded to a glass slide, sterilized with ethanol for 15 minutes, and dried thoroughly. The matrix was placed inside the perfusion chamber, then the inlet and outlet were fitted with 18-gauge needles, and finally, the top of the chamber was sealed with a glass slide. This setup allowed for fluidically sealed perfusion through the bioprinted architecture.

For matrices with designs M-C_E and M-C_EGP, GFP HUVECs were loaded into the matrix's patterned channel at a concentration of $30x10^6$ cells/mL with a 1 mL syringe. All HUVECs were between passages 7-9. Normject syringe connected to an 18-gauge flexible needle at the inlet of

the channel. The outlet was likewise catheterized with an 18-gauge flexible needle to form a fluidic seal with the channel. After injecting GFP HUVECs in suspension, cells were allowed to adhere to the bottom cylindrical surface for 15 minutes. Every 15 minutes thereafter for 6 hours, the gel was rotated by 90 degrees to establish a cylindrical coating of adhered GFP HUVECs. Any unattached cells were washed away with fresh media during the perfusion setup. Perfusion culture was maintained at five μL/min using the high precision, multi-channel peristaltic pump, ISMATEC (Cole Parmer). Tubing was connected with Luer-lock fittings from an IV media bag through the peristaltic tubing to the inlet of the perfusion chamber. Two 0.22 μm filters were placed in line with the flow before reaching the matrix – one placed right before the inlet, the second placed at a y-junction stop-cock between the media bag and the peristaltic pump. During long-term perfusion culture, media was added to the bag through this junction as needed. Before connecting to the perfusion chamber, all bubbles were evacuated by pre-wetting the tubing through to the inlet. Gelatin was injected through the endothelialized serpentine channels to form a thermo-reversible plug for M-C_EGP. For M-C_CC, GFP-HUVECs passage 5 ($5x10^6$ cells per mL, AngioProteomie) and hMSCs at passage 6 ($100x10^3$ cells per mL, Rooster Bio) were suspended in 2.5 mg/mL collagen and injected into the matrix channel.

Stitched epifluorescence images of pre-implant matrices were acquired using a Nikon Eclipse Ti inverted epifluorescent microscope (Nikon Instruments Inc., Melville, NY) with a Zyla 4.2 sCMOS camera (Andor, South Windsor, CT). The degree of overlap is specified at 30%.

2.6 *Implantation of bioprinted matrices*

All work involving animals was performed in accordance with the Guidelines for Care and Use of Laboratory Animals of Rice University and was approved by the Institutional Animal Care and Use Committee (IACUC) under protocol IACUC-21-058-RU. Groups with n = 4-5 male SCID/bg mice (6-10 weeks old, Charles River, strain code 250) underwent fat pad implantation of vascularizing gels. Briefly, mice were anesthetized with 2-4% isoflurane, and abdomens were shaved and sterilized with betadine and isopropanol. Mice received 1 mg/kg buprenorphine SR lab (Zoopharm) for pain relief and 1 mL 0.9% saline to prevent dehydration. Scalpel and scissors were used to create an incision at the linea alba and Adson forceps were used to externalize the left and right gonadal fat pads. Cell-laden matrices were gently rinsed with PBS before implantation, and the gonadal fat pads were sutured to both sides of the vascularizing matrix. Sterile 0.9% saline was used to maintain gel hydration intraoperatively. After suturing the bioprinted device to the fat pads, the gel was introduced into the abdominal cavity, and muscle and skin were closed. Mice were monitored post-operatively and provided care and husbandry as needed. Implants were explanted and evaluated at 1-, 2-, 4-, or 8-weeks post-surgery to obtain time-dependent data.

2.7 *Dextran injection, matrix explantation, fixation, and confocal imaging*

CF680-conjugated fixable dextran, 70 kDa (Biotium, Catalog #80129) was prepared at 2.5 mg/mL in PBS. 100 uL of dextran solution was injected via the tail vein 15 min prior to euthanasia. Gels were surgically explanted and photographed with a Sony A7R3 camera (Sony) and a Canon macro lens EF 100 mm 1:2.8 L IS USM (Canon). The gels were then submerged in ice-cold 4% PFA and fixed for 48h at 4°C. After fixation, gels were washed with PBS three times, 20 minutes per wash, and maintained in PBS + 0.01% sodium azide at 4°C until imaged.

Explanted matrices were imaged with Nikon A1 rsi confocal microscope using a 10X objective and 633.3 μm laser source. Laser power between 50-100% and PMT voltage between 50-150 kV was used, with a pinhole size of 122 μm. Data is presented as a maximum intensity projection of a z-stack of 11 slices. Maximum intensity projection images of fluorescent dextran acquired by confocal imaging were analyzed in FIJI. First, images were binarized to identify the fractional area occupied by the vasculature. Then, binarized images were skeletonized to determine the number of branches, junctions, and total branch length.

2.8 *Histology and immunofluorescent analysis*

Explanted and fixed matrix samples were submitted to Houston Methodist Research Institute Research Pathology Core for paraffin embedding, sectioning, and staining. The samples were sectioned at 6 μm and stained with Hematoxylin and Eosin. H&E-stained sections were imaged using Nikon A1 rsi confocal microscope with a Di-F3 color camera.

Immunofluorescence staining was performed using primary antibodies against CD31 (Abcam, ab28364 1:50) and α-SMA (Sigma A5228 1:1000), followed by secondary antibodies Goat anti-Rabbit IgG (H+L) Cross-Adsorbed Secondary Antibody, Alexa Fluor 594 (1:200 Invitrogen A11012), and Goat anti-Mouse IgG (H+L) Cross-Adsorbed Secondary Antibody, Alexa Fluor 488 (1:200 Invitrogen A11001) with MOM reagent. IF-stained slides were imaged using Nikon A1 rsi confocal microscope.

H&E-stained explant sections were imaged using a Nikon A1 rsi microscope with a Di-F3 color camera using a 40X objective. ROIs were taken of the patterned channels of the bioprinted matrix. Blood vessels were manually annotated using Adobe Illustrator, and annotated images were analyzed for the vessel semi-major axis in μm and the total number of vessels per ROI using MATLAB.

2.9 *Statistical analysis*

Statistical analyses were performed using GraphPad Prism 8 software (GraphPad Software); $*P < 0.05$, $**P < 0.01$, $***P < 0.001$, and $****P < 0.0001$. Statistical analysis of branches per mm^2, total branch length, and the fractional area was performed via one-way ANOVA with Tukey's multiple comparisons test. The analysis of vessel diameters and vessels per ROI data was performed using the Kruskal-Willis test with Dunn's multiple comparisons test.

3. Results and discussion

3.1 *Cell-laden matrix design*

Five different cell-laden matrices were designed as outlined in **Figure 1 (see methods).** We hypothesized that vascularization would be guided by the vascular cells located within patterned channels. A serpentine channel architecture was used here since it has a single inlet and a single outlet for ease of cell seeding within the patterned channel (**Supplementary Figure 1**) . Cell-laden matrices were designed by varying the following parameters: the presence of a perfusable lumen, cells in the bulk matrix, types of cells loaded into the matrix channel, and control over perioperative fluid ingress into the channel using a thermoreversible gelatin plug.

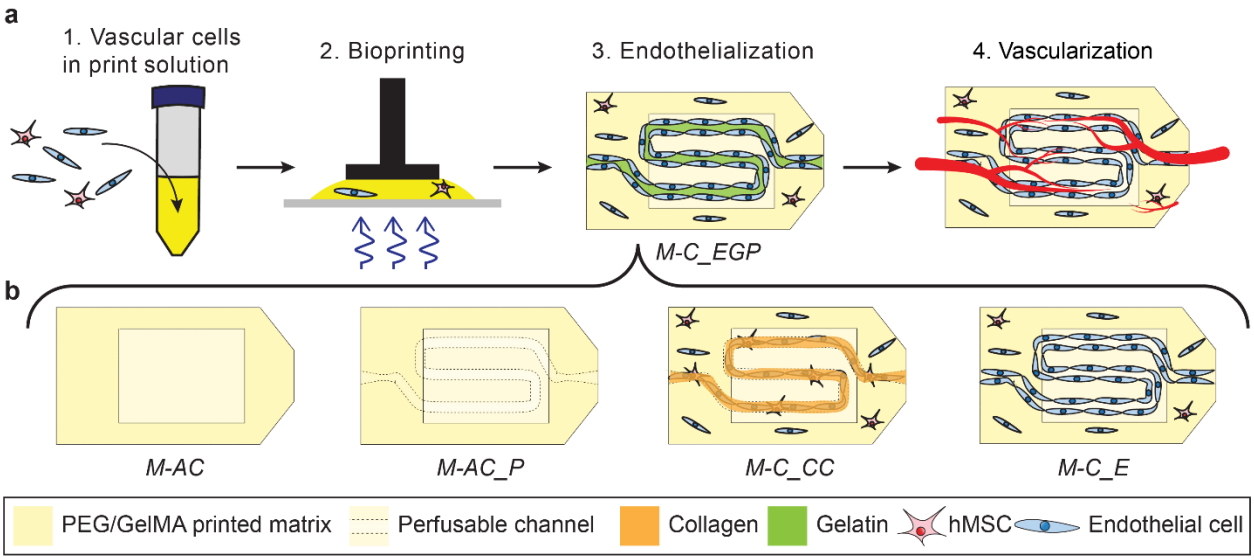

c

Matrix design	Patterned	Cells in bulk	Cells in channel	Gelatin plugs
M-AC	No	No	No	No
M-AC_P	Yes	No	No	No
M-C_CC	Yes	Yes: ECs and hMSCs	Yes: ECs and hMSCs in collagen	No
M-C_E	Yes	Yes: ECs and hMSCs	Yes: ECs under perfusion culture	No
M-C_EGP	Yes	Yes: ECs and hMSCs	Yes: ECs under perfusion culture	Yes

Fig. 1: Design of cell-laden matrices for local, patterned vascularization. (a) Cell-laden matrices are prepared and assayed as follows: matrices are bioprinted, endothelialized, and implanted for determining vascularization. (b) Multiple cell-laden matrices were designed: M-AC, M-AC_P, M-C_CC, M-C_E, and M-C_EGP. (c) Characteristics of cell-laden matrix designs. Cell-laden matrices are designed by varying the following characteristics: the presence of a serpentine channel (denoted in the patterned column in this table), cells in the bulk matrix, cells in the channels, and the presence of a gelatin plug to limit perioperative fluid ingress.

M-AC hydrogels served as a control to evaluate any angiogenic effects from hydrogel composition alone, and M-AC_P hydrogels acted as a control for hydrogel architecture because they do not contain any cells. M-C_CC, M-C_E, and M-C_EGP designs all contained a combination of ECs and hMSCs, and were evaluated because we hypothesized that vascularization would depend upon these vascular cells. M-C_CC hydrogels were used here

because of their success in prior studies (12). M-C_E and M-C_EGP designs also featured endothelialized channels and were investigated as an alternative form of endothelialized hydrogels that do not contain collagen cords. Additionally, the hMSCs printed in the bulk of these two hydrogel designs were used to assess whether bulk cells affect vascularization. Gelatin was chosen as the material for the plug in M-C_EGP hydrogels because of its thermoreversible properties and because it is similar to the gelatin-derived components of our hydrogels. We therefore expected that the gelatin plug would not have any impact on vascularization that wasn't already present from the hydrogels themselves.

3.2 *Photopolymer blends enable tunable mechanical and enzymatic degradation properties*

Biologically relevant photopolymers with cell-adhesive, degradable, and sufficiently handle-able properties were designed and synthesized as outlined in **Supplementary Figure 2**. Gelatin methacryloyl (GelMA) was chosen as a photopolymer for its cell-adhesive and degradable properties, and poly(ethylene glycol)-diacrylate (PEGDA) was chosen as a photopolymer for its ability to influence mechanical properties while maintaining matrix biocompatibility. Lithium acylphosphinate (LAP) was chosen as a photoinitiator due to its favorable cytocompatibility(37). The degree of polymer acrylation **(Supplementary Table 1)** and photopolymer storage modulus were quantified **(Supplementary Table 2)** to validate consistent chemical and physical properties across multiple batches. Furthermore, the degradability of photopolymerized droplet matrices was assayed to ensure moderate degradation rates, as implanted matrices must eventually degrade to become replaced with host tissues but must not degrade too quickly before engraftment occurs. By adding 3.25% 3.4 kDa PEGDA to 10% GelMA, collagenase degradation took 4-fold longer, demonstrating tunable degradation properties **(Supplementary Figure 3b).** A similar balance exists with respect to gel mechanics, as gels must be stiff enough to surgically manipulate but soft enough to integrate into the body and maintain biocompatibility. Using previous studies as a guide (29), we examined the mechanical benefits of adding PEGDA to GelMA in specific quantities. The addition of 3.25% 3.4 kDa PEGDA to 10% GelMA produced a 3-fold increase in matrix storage modulus **(Supplementary Figure 3c)** as measured using a parallel plate rheometer during UV exposure, resulting in a surgically handle-able gel. These data suggested that the matrix formulation of 10% GelMA with 3.25% 3.4 kDa PEGDA can satisfy degradation and mechanical requirements and was used for the remaining studies in this work.

3.3 *Laminar flow observed within channels of bioprinted matrices*

Given that matrices M-C_E and M-C_EGP were designed for perfusion culture of ECs, we sought to validate fluid dynamics within the patterned channels. ECs are known to respond to wall shear stress within vessels, demonstrating flow-based activation (34-36). Consistent wall shear stress can be achieved by laminar flow. Given the smooth internal channel surfaces attained with SLATE bioprinting, we hypothesized that laminar flow would occur within the channels.

Acellular matrices were printed with a serpentine channel using bioprinting techniques developed in prior studies to study fluid dynamics within the patterned channel. Fluorescent beads were mixed at a low concentration with PBS and perfused through the printed matrix lumens. By tracking the movement of tracer fluorescent beads under fluorescent microscopy video capture via

particle imaging velocimetry (PIV), the positions of individual beads could be tracked over time, allowing for fluid dynamics analysis.

Equation 1: $Re = \frac{VD\rho}{\mu}$

Where V = fluid velocity (m * s^{-1}), D = characteristic length, in this case vessel diameter (m), ρ = fluid density (kg * m^{-3}), and μ = fluid dynamic viscosity (kg * m^{-1} * s^{-1}). (42)

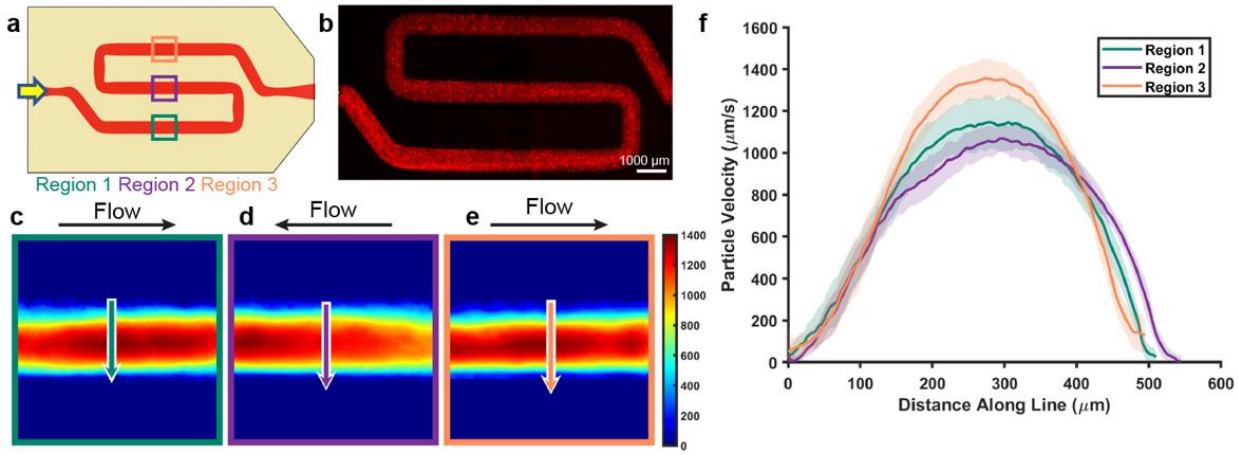

Fig. 2: Fluid dynamics within the serpentine vessel. (a) Acellular matrices with serpentine channels were prepared. (b) Fluorescent beads were perfused through the inlet of the channel to determine velocity profiles using particle imaging velocimetry (PIV) (scale = 1000 μm). (c-e) Particle velocities are shown in μm/s for Region 1, Region 2, and Region 3. (f) Velocity profiles were quantified for each of the ROIs in (c-e) of the same matrix and plotted over a cross-section through the matrix (mean +/- s.d.). Differences between flow profiles can most likely be attributed to slight heterogeneities along the length of the channel, which affect fluid velocity.

A parabolic-shaped flow profile was observed at three different positions in the matrix, characteristic of laminar flow dynamics. The maximum observed particle velocity of 1400 μm/s, vessel diameter of 700 μm, and appropriate density and dynamic viscosity of water at 37°C correspond to a Reynolds number of 14.2, which is well within the accepted range for laminar flow (42). These findings validated our hypothesis about attaining laminar flow within these bioprinted channels and encouraged us to proceed with this serpentine design for future experiments, including channel endothelialization.

3.4 *Channel endothelialization and cell-cell coordination with cell-loaded matrices*

To ensure the successful fabrication of designed constructs, we evaluated whether ECs could maintain adherence and viability within perfusable channel lumens and if they could associate with each other. We hypothesized that the cell-adherent nature of the GelMA-containing matrix would allow EC adhesion along the perfusable lumens, and that ECs would be able to maintain viability due to favorable matrix conditions and direct access to the cell culture medium. We also hypothesized that ECs would be able to begin associating with each other within the matrix due to the MMP-degradable nature of GelMA (38) and the ability of MSCs to help stabilize newly formed tubules (20, 21).

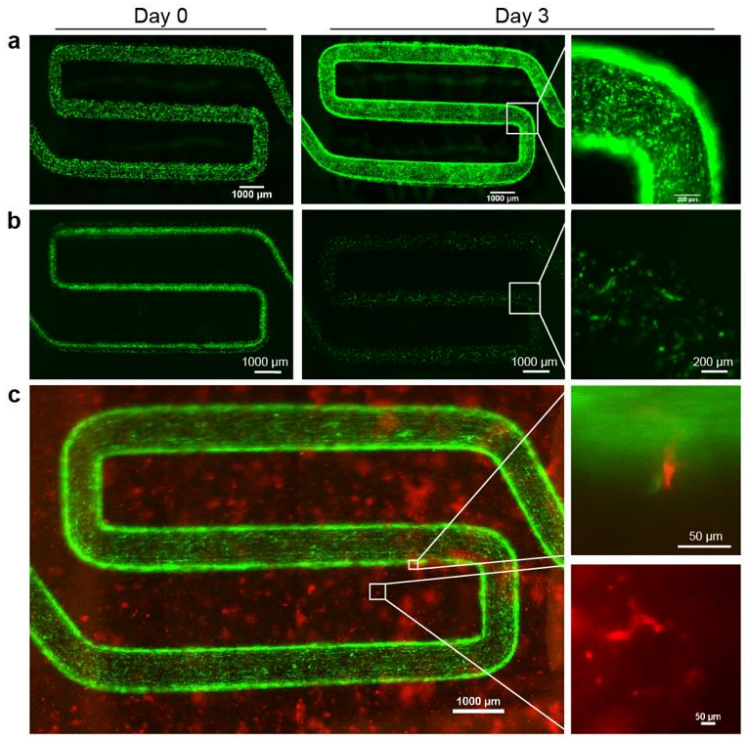

Fig. 3: Endothelialization of patterned channels and cell-cell coordination. (a) After injecting endothelial cells and rotating for six hours, fluorescent endothelial cells are seen within the serpentine channel (Day 0, scale = 1000 µm). After three days of perfusion culture, endothelial cells line the vessel walls, forming uniform, endothelialized channels (Day 3, scale = 1000 µm, inset scale = 200 µm). (b) A similar period without perfusion results in sparse endothelial cell coverage within the channels (Day 0 and Day 3 scale = 1000 µm, Day 3 inset scale = 200 µm). (c) Matrices with RFP HUVECs and unlabeled hMSCs bioprinted into the bulk matrix were endothelialized and maintained under perfusion culture for three days (scale = 1000 µm). Cellular coordination between cells in the channel and those in the bulk matrix was observed (panel c, upper inset, scale = 50 µm). Cellular coordination in the matrix was observed (panel c, lower inset, scale = 50 µm).

Bioprinted lumens were endothelialized and maintained under perfusion culture **(Fig. 3a)**. ECs were seen throughout the serpentine channel after initial injection and rotational seeding on day 0. After three days of perfusion culture, endothelial cells had spread across the interior of the channels of the bioprinted matrix **(Fig. 3a)**. When matrices were maintained in static conditions without perfusion culture, endothelial cells had poor adherence resulting in an inhomogeneous, patchy

channel lining **(Fig. 3b)**, demonstrating the necessity for perfusion culture maintenance of endothelial cells. We noted that ECs maintained viability of over 85% in perfusion-cultured matrices, meeting the FDA requirement of greater than 70% viability for cell-based therapies **(Supplementary Figure 5)**(43-45).

Furthermore, matrices with RFP HUVECs and unlabeled hMSCs bioprinted in the bulk matrix were endothelialized with GFP HUVECs and maintained under perfusion culture **(Fig. 3c)**. Co-culture matrices demonstrated coordination between ECs in the channel and bulk and cellular coordination within the bulk matrix **(Fig. 3c)**. Based on the mechanics of sprouting angiogenesis (46) and the ability of endothelial cells to undergo tubulogenesis in GelMA-based hydrogels (21), we hypothesize that this coordination is the result of putative angiogenesis. Overlapping GFP and RFP signals further suggests that endothelial cells have begun to degrade their local environment in the matrix and begin associating with each other. These are critical elements needed for vessel formation via tubulogenesis and factors essential for vascular invasion (20, 21, 38). These studies verified that endothelial cells could successfully adhere to these matrices and begin to associate with each other.

3.5 *Cellularized bioprinted matrices demonstrate the highest vascularization in vivo*

A key focus was determining whether cell-laden matrices could engraft and vascularize *in vivo*. The five designed cell-laden matrices were prepared and sutured to the gonadal fat pads of SCID/bg mice **(Supplementary Figure 6)**, an implant site chosen due to its high angiogenic capacity (27). Eight weeks after implantation, fluorescent dextran was administered intravenously to enable the detection of blood vessels **(Fig. 4a-c)**. **(Supplementary Figure 7)**. CF680 dextran spectral fingerprint was identified in acellular matrices and explanted samples via multi-spectral imaging **(Supplementary Figure 8),** validating that the observed fluorescent signal matched the spectrum of the injected fluorophore. An image analysis pipeline **(Supplementary Figure 9)** was used to quantify key vascular parameters, including the fractional area (pixels occupied by vasculature), branches per mm^2, and total branch length (27).

Upon retrieval, multiple encouraging vascular features were seen in the explanted matrices. First, matrix remodeling was observed *in vivo* via degradation and matrix softening, most notably in groups M-C_E and M-C_EGP **(Fig. 4b)**. These two groups had bulk vascular cells and endothelialized channels maintained under perfusion culture, which may have activated the endothelial cell populations more than other groups. We also noticed that the gonadal fat pads were firmly adhered to the implanted matrix even after removing sutures, demonstrating the integration of the engineered tissue into the host **(Fig. 4b)**.

Matrices with design M-C_E were seen to have the highest degree of vascularization across all three metrics compared to other designs investigated in this study **(Fig. 4c-f).** Matrices with design M-C_E had significantly greater fractional area than those with M-AC, M-AC_P, and M-C_CC ($p < 0.05$), with 1.2-8.9% of the total image area occupied by the vasculature. The mean fractional area occupied by the vasculature for M-C_E was 3.775%, which is over 6-fold higher than M-C_EGP, which had a mean fractional area of 0.6275%, and over 21-fold higher than M-C_CC, which had a mean fractional area 0.1725%, demonstrating that the vascularization of M-C_E matrices was greatest relative to other groups. This finding highlighted the importance of perfusion culture to properly activate endothelial cells relative to M-C_CC, which did not have perfusion cultured endothelial cells. This also may reflect the effect of perioperative fluid ingress into the channels, as M-C_E had greater vascularization across the various parameters. We did not observe remaining GFP or RFP signal in explanted matrices, highlighting that the vasculature was

comprised of host cells. Ultimately, this study demonstrates the potential for the pre-patterned endothelialized channels to influence the development of patterned vasculature *in vivo.*

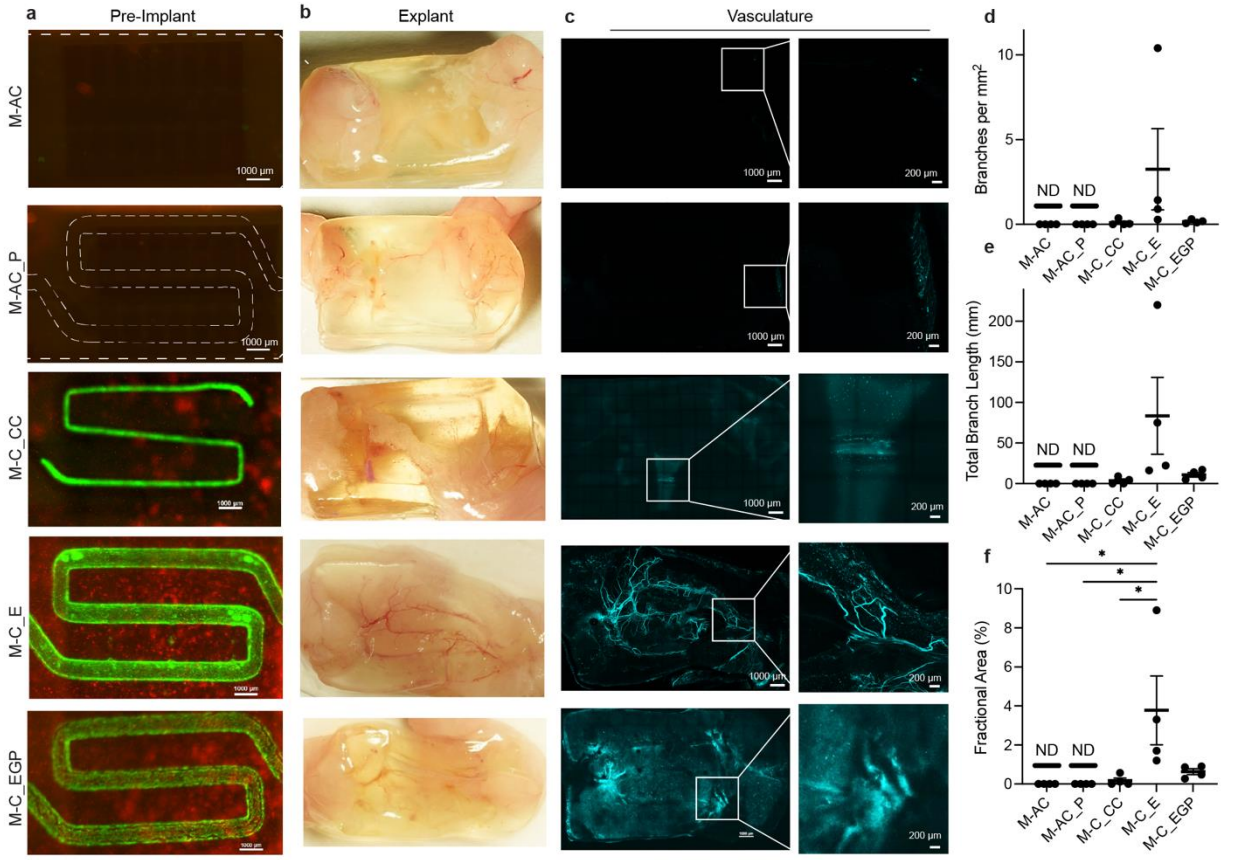

Fig. 4: Comparison of in vivo angiogenesis across multiple biomaterial designs at eight weeks. (a) Epifluorescent imaging of bioprinted matrices before implantation (scale = 1000 µm). (b) Gross vascular morphology and matrix degradation via macro-imaging photography. (c) Intravenously administered fixable, fluorescent dextran allowed for visualization of construct vascularization (scale 1000 µm, inset scale 200 µm). (d) Quantification of branches per mm^2, (e) total branch length, and (f) the fractional area occupied by vasculature was performed by analyzing confocal images. n = 4-5 per group, data shown as mean +/- s.e.m. *$p < 0.05$, **$p < 0.01$, ***$p < 0.001$, and **** $p < 0.0001$. ND = not detected.

Our observation of cell-cell association in the matrix **(Fig. 3c)** and the dependence of matrix engraftment upon the presence of ECs and MSCs **(Fig. 4b-f)** aligns with the conclusions of prior studies (38). Perfusion culture of endothelial cells is also known to upregulate an angiogenic phenotype (34) and may have influenced the improved vascularization of design M-C_E over non-perfusable M-C_CC **(Fig. 4b-f)**. In these ways, our findings were aligned with the conclusions of prior studies in this field. Notably, explanted M-C_E hydrogels sometimes displayed vasculature that vaguely resembled the shape of the patterned channel (**Fig. 4c**). Native angiogenic processes

would not likely form vascular structures in such a serpentine shape, so we interpret this observation as evidence of guided vascular formation.

3.6 *Patterned vascularization in matrix channels develops from two to eight weeks post-implantation*

Fast and durable vascularization is essential to ensure engineered tissues maintain viability and functionality without prolonged initial hypoxia. Because M-C_E matrices displayed the greatest extent of vascularization in previous studies, we prepared for a new set of mouse experiments using this design. These matrices were implanted *in vivo* using the same procedure as in previous vascularization experiments and then explanted at one, two, four, and eight weeks. Histological analysis was performed to visualize the degree of vascularization by quantifying vessel diameter, vessel density, and the vascular phenotype on a cellular level via immunohistochemistry.

Host tissues were observed to integrate with the engineered tissue with increased vascular density and diameter over time. From two weeks onwards, 5-15 μm diameter vessels were apparent in histological sections, evidenced by flattened circumferential endothelial cells and biconcave red blood cells within the blood vessel lumens **(Fig. 5c)**. Vessels with diameters over 100 μm, on the scale of arterioles and venules, were observed at the eight-week time point **(Fig. 5c,d)**. The presence of these larger diameter vessels is highly encouraging, demonstrating the complexity of vasculature developing within these engineered constructs. The mean density of vasculature within ROIs of the printed channels increased over time, from a mean value of 4.286 vessels per ROI at two weeks to 12.22 and 16.22 vessels per ROI at four and eight weeks. At eight weeks, the mean vessel density was 1.33-fold greater than at four weeks and 3.78-fold greater than at two weeks, highlighting increasing vascularization over time in these constructs. Furthermore, immunohistochemistry was utilized to determine whether vessels had matured to determine the presence of endothelial cells (CD31) and pericytes (αSMA). The presence of CD31+ and αSMA+ vessels demonstrated maturation of vessels within these bioprinted constructs, as pericyte association is one of the last steps in the angiogenesis process (**Fig. 5f)**.

In a therapeutic context, enhanced vascularization is widely explored for Type 1 diabetes cell therapy, having been demonstrated to be essential for metabolically demanding pancreatic islets (47). Cell therapies can be designed to have smaller constructs and thus may be near-term beneficiaries from approaches to enhance vascularization. In the long term, fabricating larger and more complex organs will depend upon forming an increasingly complex vascular system. Key to achieving these goals is the formation of larger vessels. Once larger vessels have been formed, capillaries can sprout to perfuse the engineered tissue (48). However, expanding applications to islet encapsulation for diabetes cell therapies would likely require more materials optimization, as the degradability of our PEGDA-GelMA formulation may not be ideal for islet survival. Many non-patterning approaches with some patterning approaches are limited by seemingly creating microvasculature. Similar to this work, Szklanny et al (48) demonstrate the importance of biomaterial patterning to guiding large vessel development *in vivo*. An alternative approach for achieving large vessel formation is demonstrated by Zhang et al (49) where endothelialized channels served as functional conduits after surgical anastomosis to host vasculature. While the approach used by Zhang et al can create complex vascular architectures like SLATE bioprinting, this technique is currently limited by low vessel circularity, which may hinder future applications.

While this work demonstrates vascularization with cell-laden matrices, successful translation of this approach may require autologous-derived cells such as iPSCs or implantation in immunosuppressed individuals. iPSC-derived endothelial cells have been developed and utilized

for vascularization, demonstrating their utility for this application (6). Alternatively, immunosuppression would likely require a similar regimen utilized for recipients of donated organs. Studies have shown that non-host ECs are replaced by host ECs over time within implanted materials (12), suggesting that immunosuppression may only need to be transiently delivered.

Cell-laden matrices can enable engraftment and guidance of large vessels *in vivo*. The modular design of this approach can allow for application-dependent tuning of matrix properties. Implantable cell-based therapies have been evaluated in the intraperitoneal space in large animal models and NHPs (50), highlighting future translational potential. The following steps in evaluating these vascularizing matrices would be to utilize them to enhance pancreatic islets' engraftment for Type 1 diabetes cell therapy, specifically to evaluate their ability to restore normoglycemia in preclinical models. These findings can have broad implications for the development of new engineered tissues.

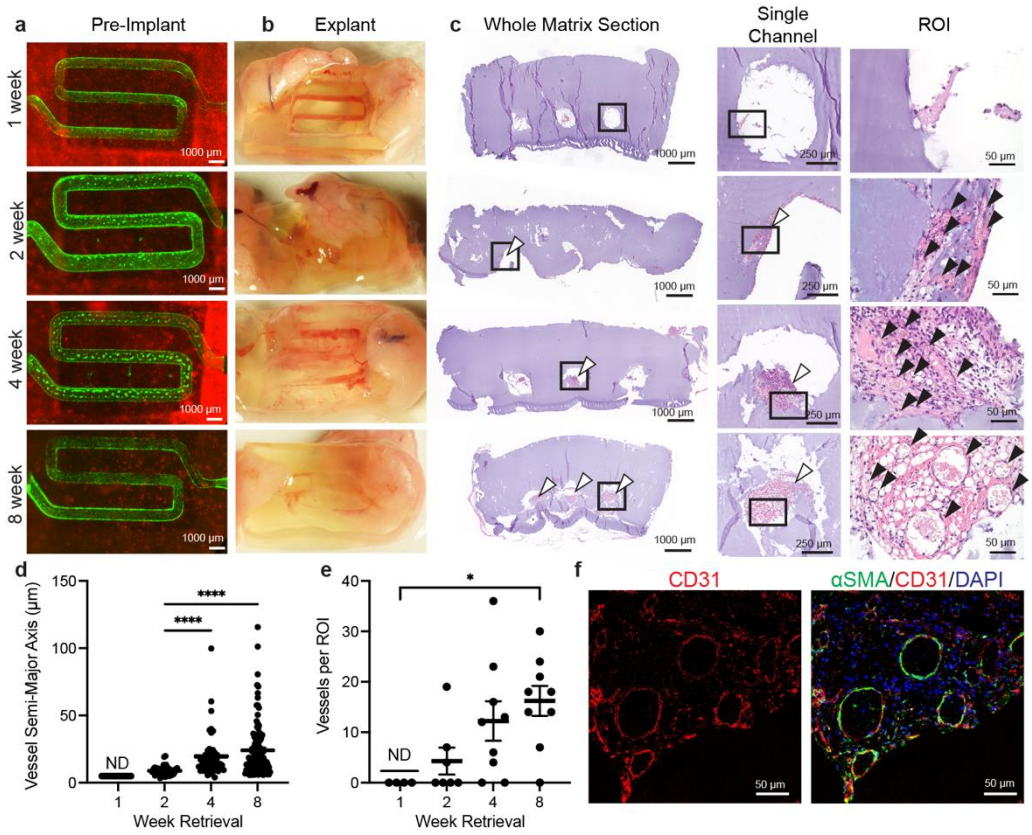

Fig. 5: Temporal kinetics of vascular network development within patterned and cellularized matrices. (a) Epifluorescent imaging of matrices prior to implantation (scale = 1000 µm). (b) Gross morphology of explanted matrices. (c) H&E-stained matrix sections (Matrix section, scale = 1000 µm, Single Channel scale = 250 µm, ROI scale = 50 µm). (d) Vessel semi-major axis (e) and vessels per ROI were quantified. (f) Immunofluorescent staining for CD31 (red) and αSMA (green), with DAPI counterstain (blue) for 8-week retrieval (scale = 50 µm) (f). n = 4-5 per group. Data presented as mean +/- s.e.m. *p < 0.05, **p< 0.01, ***p < 0.001, and **** p < 0.0001. ND = not detected.

4. Conclusion

The development of vascularized tissue-engineered constructs is essential to meeting the clinical needs in organ transplantation. The development of patterned vasculature with large (>100 μm) vessels is critical for ensuring effective nutrient delivery throughout metabolically active tissues. This study determined that bioprinted cell-laden matrices can enable local patterned vascularization, notably with vessels primarily localized within pre-patterned channels and the formation of large vessels (>100 μm) within these matrices *in vivo*. Laminar flow was detected in the perfusable channel at multiple locations, essential for consistent wall shear stress for flow-based EC activation. Under perfusion culture, ECs maintained adhesion to bioprinted channels, had >70% viability, and cell-cell coordination was observed at the channel-bulk interface and within the bulk matrix, demonstrating local degradability and the ability for cells to interact with each other. Vascularization was greatest for cell-laden matrices with perfusion-cultured endothelial cells relative to non-perfusable designs. Finally, vascularization was seen to develop as soon as two weeks and further developed throughout an 8-week duration in these matrices, demonstrating durable vascular development. Of note was the presence of large-scale vessels that developed within these hydrogels. This study demonstrates the potential for bioprinted cell-laden matrices to serve as a versatile element of future engineered tissues and cell therapies.

Author Contributions:
Conceptualization: S.P., G.A.C, S.M., and O.V. Methodology: S.P., G.A.C, S.M., M.D.D., Z.Y., D.W.S., and O.V. Investigation: S.P., G.A.C, K.D.J., S.M., M.D.D., Z.Y., D.W.S., and O.V. Visualization: S.P., G.A.C., K.D.J., D.W.S., and O.V. Project administration: S.P., S.M., and O.V. Supervision: O.V. Writing—Original draft: S.P., G.A.C., K.D.J., S.M., A.K.M., and O.V. Writing—Review and editing: S.P., G.A.C, K.D.J., S.M., A.K.M., M.D.D., Z.Y., D.W.S., and O.V.

Competing Interest Statement: S.P., S.M., D.W.S., and O.V. are inventors on PCT Application No. PCT/US2020/018511 "Vascularizing Devices and Methods for Implanted Diagnostics and Therapeutics," Feb 17, 2020.

Acknowledgments

This work was supported by the Juvenile Diabetes Research Foundation (Grant 1-PNF-2018-662-S-B) and the National Institutes of Health (Grant R01DK120459). We thank the many open-source and related projects that facilitated this work, including Arduino.cc, Blender.org, and Openscad.org. We thank Jordan Miller, Bagrat Grigoryan, and Ian Kinstlinger for their helpful discussions and their establishment of core methodologies utilized throughout this work. We thank A. Budi Utama at the Rice University Shared Equipment Authority for his guidance. Some figure panels were generated using Biorender.com.

References

1. Langer R, Vacanti JP. Tissue engineering. Science. 1993;260(5110):920-6.
2. Lanza R, Langer R, Vacanti J, Atala A. eds. Principles of Tissue Engineering. 5 ed: Academic Press; 2020.
3. Shirure VS, Hughes CCW, George SC. Engineering Vascularized Organoid-on-a-Chip Models. Annual Review of Biomedical Engineering. 2021;23(1):141-67.
4. Grebenyuk S, Ranga A. Engineering Organoid Vascularization. Frontiers in Bioengineering and Biotechnology. 2019;7.
5. Administration HRS. Organ Donation Statistics 2022 [updated March 2022. Available from: https://www.organdonor.gov/learn/organ-donation-statistics.
6. Wiegand C, Banerjee I. Recent advances in the applications of iPSC technology. Current Opinion in Biotechnology. 2019;60:250-8.
7. O'Connor C, Brady E, Zheng Y, Moore E, Stevens KR. Engineering the multiscale complexity of vascular networks. Nature Reviews Materials. 2022;7:702-16.
8. Carmeliet P, Jain RK. Angiogenesis in cancer and other diseases. Nature. 2000;407(6801):249-57.
9. Miller JS, et al. Rapid casting of patterned vascular networks for perfusable engineered three-dimensional tissues. Nature Materials. 2012;11(9):768-74.
10. Skylar-Scott MA, et al. Biomanufacturing of organ-specific tissues with high cellular density and embedded vascular channels. Science Advances. 2019;5(9):eaaw2459.
11. Fleischer S, Tavakol DN, Vunjak-Novakovic G. From Arteries to Capillaries: Approaches to Engineering Human Vasculature. Advanced Functional Materials. 2020;30(37).
12. Baranski JD, et al. Geometric control of vascular networks to enhance engineered tissue integration and function. Proceedings of the National Academy of Sciences of the United States of America. 2013;110(19):7586-91.
13. Mirabella T, et al. 3D-printed vascular networks direct therapeutic angiogenesis in ischaemia. Nature Biomedical Engineering 2017 1:6: Nature Publishing Group; 2017. p. 1-8.
14. Song W, et al. Engineering transferrable microvascular meshes for subcutaneous islet transplantation. Nature Communications. 2019;10(1):4602.
15. Murray CD. The Physiological Principle of Minimum Work. Proceedings of the National Academy of Sciences. 1926;12(3):207-14.
16. Sherman TF. On connecting large vessels to small. The meaning of Murray's law. Journal of General Physiology. 1981;78(4):431-53.
17. McCulloh KA, Sperry JS, Adler FR. Water transport in plants obeys Murray's law. Nature. 2003;421(6926):939-42.
18. An Y, et al. Autophagy promotes MSC-mediated vascularization in cutaneous wound healing via regulation of VEGF secretion. Cell Death & Disease. 2018;9(2):1-14.
19. Ghajar CM, Blevins KS, Hughes CCW, George SC, Putnam AJ. Mesenchymal Stem Cells Enhance Angiogenesis in Mechanically Viable Prevascularized Tissues via Early Matrix Metalloproteinase Upregulation. Tissue Engineering. 2006;12(10):2875-88.
20. Moon JJ, et al. Biomimetic hydrogels with pro-angiogenic properties. Biomaterials. 2010;31(14):3840-7.
21. Calderon GA, et al. Tubulogenesis of co-cultured human iPS-derived endothelial cells and human mesenchymal stem cells in fibrin and gelatin methacrylate gels. Biomaterials Science. 2017;5(8):1652-60.

22. Converse JM, Smahel J, Smahel J, Ballantyne DL, Harper AD. Inosculation of vessels of skin graft and host bed: A fortuitous encounter. British Journal of Plastic Surgery. 1975;28(4):274-82.
23. Laschke MW, et al. Short-Term Cultivation ofIn SituPrevascularized Tissue Constructs Accelerates Inosculation of Their Preformed Microvascular Networks After Implantation into the Host Tissue. Tissue Engineering Part A. 2011;17(5-6):841-53.
24. Vlahos AE, Talior-Volodarsky I, Kinney SM, Sefton MV. A scalable device-less biomaterial approach for subcutaneous islet transplantation. Biomaterials. 2021;269:120499.
25. Coindre VF, Kinney SM, Sefton MV. Methacrylic acid copolymer coating of polypropylene mesh chamber improves subcutaneous islet engraftment. Biomaterials. 2020;259:120324.
26. Vlahos AE, et al. Endothelialized collagen based pseudo-islets enables tuneable subcutaneous diabetes therapy. Biomaterials. 2020;232:119710.
27. Weaver JD, et al. Vasculogenic hydrogel enhances islet survival, engraftment, and function in leading extrahepatic sites. Science Advances. 2017;3(6):e1700184.
28. Redd MA, et al. Patterned human microvascular grafts enable rapid vascularization and increase perfusion in infarcted rat hearts. Nature Communications. 2019;10(1):584.
29. Grigoryan B, et al. Multivascular networks and functional intravascular topologies within biocompatible hydrogels. Science. 2019;364(6439):458-64.
30. Kinstlinger IS, et al. Perfusion and endothelialization of engineered tissues with patterned vascular networks. Nature Protocols. 2021:1-25.
31. Grigoryan B, et al. Development, characterization, and applications of multi-material stereolithography bioprinting. Scientific Reports. 2021;11(1):3171.
32. Corbett DC, et al. Thermofluidic heat exchangers for actuation of transcription in artificial tissues. Science Advances. 2020;6(40):eabb9062.
33. Yue K, et al. Synthesis, properties, and biomedical applications of gelatin methacryloyl (GelMA) hydrogels. Biomaterials. 2015;73:254-71.
34. dela Paz NG, Walshe TE, Leach LL, Saint-Geniez M, D'Amore PA. Role of shear-stress-induced VEGF expression in endothelial cell survival. Journal of Cell Science. 2012;125(4):831-43.
35. Conklin BS, Zhong D-s, Zhao W, Lin PH, Chen C. Shear Stress Regulates Occludin and VEGF Expression in Porcine Arterial Endothelial Cells. Journal of Surgical Research. 2002;102(1):13-21.
36. Rashdan NA, Lloyd PG. Fluid shear stress upregulates placental growth factor in the vessel wall via NADPH oxidase 4. American Journal of Physiology-Heart and Circulatory Physiology. 2015;309(10):H1655-H66.
37. Fairbanks BD, Schwartz MP, Bowman CN, Anseth KS. Photoinitiated polymerization of PEG-diacrylate with lithium phenyl-2,4,6-trimethylbenzoylphosphinate: polymerization rate and cytocompatibility. Biomaterials. 2009;30(35):6702-7.
38. Miller JS, et al. Bioactive hydrogels made from step-growth derived PEG–peptide macromers. Biomaterials. 2010;31(13):3736-43.
39. Shirahama H, Lee BH, Tan LP, Cho N-J. Precise Tuning of Facile One-Pot Gelatin Methacryloyl (GelMA) Synthesis. Scientific Reports. 2016;6(1).
40. Arcaute K, Mann BK, Wicker RB. Stereolithography of Three-Dimensional Bioactive Poly(Ethylene Glycol) Constructs with Encapsulated Cells. Annals of Biomedical Engineering. 2006;34(9):1429-41.

41. Kinstlinger IS, et al. Generation of model tissues with dendritic vascular networks via sacrificial laser-sintered carbohydrate templates. Nature Biomedical Engineering. 2020;4(9):916-32.
42. Reynolds O. IV. On the dynamical theory of incompressible viscous fluids and the determination of the criterion. Philosophical Transactions of the Royal Society of London (A). 1894;186:123-64.
43. Administration USDoHaHSFaD. Q12 Technical and Regulatory Considerations for Pharmaceutical Product Lifecycle Management Annexes Guidance for Industry. 2021. p. 27.
44. Administration USDoHaHSFaD. Guidance for Industry Biologics License Applications for Minimally Manipulated, Unrelated Allogeneic Placental/Umbilical Cord Blood Intended for Hematopoietic and Immunologic Reconstitution in Patients with Disorders Affecting the Hematopoietic System. 2014:48.
45. Administration USDoHaHSFaD. Guidance for FDA Reviewers and Sponsors. In: Administration USDoHaHSFaD, editor. 2008. p. 36.
46. Li A, Dubey S, Varney ML, Dave BJ, Singh RK. IL-8 Directly Enhanced Endothelial Cell Survival, Proliferation, and Matrix Metalloproteinases Production and Regulated Angiogenesis. The Journal of Immunology. 2003;170(6):3369-76.
47. Bowers DT, Song W, Wang L-H, Ma M. Engineering the vasculature for islet transplantation. Acta Biomaterialia. 2019;95:131-51.
48. Szklanny AA, et al. 3D Bioprinting of Engineered Tissue Flaps with Hierarchical Vessel Networks (VesselNet) for Direct Host-To-Implant Perfusion. Advanced Materials. 2021;33(42).
49. Zhang B, et al. Biodegradable scaffold with built-in vasculature for organ-on-a-chip engineering and direct surgical anastomosis. Nature Materials. 2016;15(6):669-78.
50. Bochenek MA, et al. Alginate encapsulation as long-term immune protection of allogeneic pancreatic islet cells transplanted into the omental bursa of macaques. Nature Biomedical Engineering. 2018;2(11):810-21.